Ninth International Conference on CFD in the Minerals and Process Industries
CSIRO, Melbourne, Australia
10-12 December 2012

SIMULATION OF SORPTION ENHANCED STEAM METHANE REFORMING AND CHEMICAL LOOPING REFORMING IN A CIRCULATING FLUIDIZED BED REACTOR

Rafael A. SÁNCHEZ* **and Hugo A. JAKOBSEN**

Department of Chemical Engineering, Norwegian University of Science and Technology, Trondheim 7034, NORWAY
*Corresponding author, E-mail address: rafael.sanchez@chemeng.ntnu.no

ABSTRACT

This work studies the potential of a circulating fluidized bed reactor (CFBR) one dimensional model for two reforming processes, Sorption-Enhanced Steam Methane Reforming (SE-SMR) and Chemical Looping Reforming (CLR). The model solves the full governing equations, which is an improvement from the conventional Kunii-Levenspiel type of models. Those models consider a stagnant solid phase, clearly inadequate for these dynamic processes with carryover of solid particles.
After the processes are explained and the model described, a few results are shown for a SE-SMR case. The results are compared against experiments from the literature, and they are found to be in good agreement.

NOMENCLATURE

a_s	Interfacial area per unit volume
cal	Calciner unit, regenerator unit
Cp	Specific heat capacity at constant pressure
d	Unit diameter
d_p	Particle diameter
f_g, f_p	Friction factor with the wall
g	Gravity, gas phase
h, h_{bed}	Heat transfer coefficient
i	Species
k	Phase
M_i	Molecular weight of species i
MO	Metal Oxide
OC	Oxygen Carrier
p	pressure, particle, solid phase
r	Reaction rate
ref	Reformer unit
T	Temperature
T_p'	Temperature of incoming solids
t	Time
v	Velocity
z	Axial coordinate
α	Volume fraction
β	Interfacial momentum transfer coefficient
λ	Thermal conductivity
ΔH_r	Enthalpy of reaction
λ_{sc}	Volumetric sorbent to catalyst ratio
Γ	Net mass source of solids from the other unit
η_{CO2}	CO_2 capture efficiency
μ, μ_{eff}	Laminar and effective viscosity
ν	Stoichiometric coefficient
ρ	Density
ω_i	Mass fraction of species i
ω_i'	Mass fraction of species i, incoming solids

INTRODUCTION

Interest in technologies that allow reducing greenhouse gas emissions has surged in the last years. The SE-SMR and CLR processes can operate in CFBRs. In a CFB reactor the solid particles used in one of the units for the reforming process are exchanged to the second unit. There the particles are regenerated and sent back to the first unit, thus allowing continuous operation.
Both the SE-SMR and the CLR processes feature CO_2 separation. These processes produce synthesis gas, which can be used for energy production and feedstock supply.
In the SE-SMR process, the CFBR consists of a reformer unit and a decarbonator unit. The reforming of natural gas to hydrogen proceeds as the conventional SMR in the reformer unit, but enhanced by using a solid CO_2 sorbent MO, which acts shifting the equilibrium towards more production of H_2.
Typically, the sorbent is a calcined calcium carbonate such as dolomite or limestone, although there is growing research in synthetic sorbents with improved performance, though with a down side being their higher costs.
The SE-SMR process consists of the following reactions:

$$CH_4 + H_2O \rightarrow CO + 3H_2 \quad (1)$$
$$CO + H_2O \rightarrow CO_2 + H_2 \quad (2)$$
$$CH_4 + 2H_2O \rightarrow CO_2 + 4H_2 \quad (3)$$
$$MO + CO_2 \rightarrow MCO_3 \quad (4)$$

In addition to the sorbent, a catalyst is still needed to lower the energy barriers of the reforming reactions 1 to 3. Typical hydrogen conversion yields are above 95% expressed as a dry mole fraction. One of the main advantages of this process is that virtually pure CO_2 can be obtained from the decarbonator unit, permitting subsequent transport and storage in geological formations without further separation stages.
In the CLR process the CFBR is made up of an Air Unit (AU) and a Fuel Unit (FU). In the AU, air is fed and solid particles are oxidized as follows:

$$M + 1/2\ O_2 \rightarrow MO \quad (5)$$

Oxidized solids circulate to the FU where the following reactions take place:

$$CH_4 + 4MO \rightarrow 4M + CO_2 + 2H_2O \quad (6)$$
$$H_2 + MO \rightarrow H_2O + M \quad (7)$$

$$CO + MO \rightarrow CO_2 + M \quad (8)$$

In addition to the reactions (6) to (8), reforming reactions (1) to (3) also occur in the Fuel Unit, as long as there is a catalyst present such as Ni. Ni-compounds are thus promising for the CLR process, though the catalysing properties of oxygen carriers are poorer compared to those for commercial Ni catalysts, due to different powder preparation and consequent structural properties. In this sense, more research is needed before CLR can be understood in the same level as conventional SMR.

MODEL DESCRIPTION

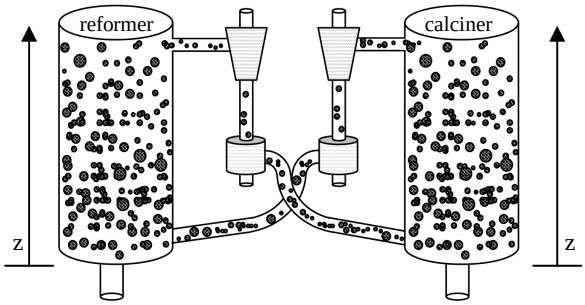

Figure 1: Schematic drawing of the CFBR. The governing equations are discretized in the axial coordinate, z. The connexions between the units are modelled by the source terms in Equations (15) and (16). Cyclones at the outlet of each unit separate gas from solids. In this work the cyclones are assumed to have efficiency 1.

Conventional models for gas-solid multiphase reactive flows in fluidized systems like the Kunii-Levenspiel three phase model and the Davidson-Harrison or the Van Deemter two-phase models assume a stagnant distribution of solids. This assumption is not valid in a CFBR since the solids are exchanged between the units, and thus solid mass fluxes need to be calculated. Furthermore, dynamic calculations imply changing properties such as species composition and density. Therefore the governing equations need to be solved without the stagnant solid assumption in order to model the physical problem in a realistic manner. Figure 1 shows a schematic drawing of the CFBR modelled.

Governing Equations

The Reynolds-averaged 1D governing equations of momentum, mass, energy and species mass fractions are discretized over a staggered grid arrangement with the Finite Volume Method (Jakobsen, 2008). The discretized equations are solved in Matlab. The governing equations for gas phase are the following:

Gas phase mass balance

$$\frac{\partial}{\partial t}\left(\alpha_g\rho_g\right)+\frac{\partial}{\partial z}\left(\alpha_g\rho_g v_g\right)=\sum_j r_j \sum_{i\in g} \nu_{i,j}M_i \quad (9)$$

Gas phase momentum balance

$$\frac{\partial}{\partial t}\left(\alpha_g\rho_g v_g\right)+\frac{\partial}{\partial z}\left(\alpha_g\rho_g v_g v_g\right)=-\alpha_g\frac{\partial p_g}{\partial z}+\frac{\partial}{\partial z}\left(\alpha_g\mu_g^{eff}\frac{\partial v_g}{\partial z}\right) \quad (10)$$
$$-\alpha_g\rho_g g+\beta\left(v_p-v_g\right)-\frac{2f_g\alpha_g\rho_g|v_g|v_g}{d}$$

Gas phase energy balance

$$\left(\frac{\partial T_g}{\partial t}+v_g\frac{\partial T_g}{\partial z}\right)\alpha_g\rho_g Cp_g=\frac{\partial}{\partial z}\left(\alpha_g\lambda_g\frac{\partial T_g}{\partial z}\right)+a_s\alpha_p h\left(T_p-T_g\right) \quad (11)$$

Gas phase species mass fractions

$$\frac{\partial}{\partial t}\left(\alpha_g\rho_g\omega_i\right)+\frac{\partial}{\partial z}\left(\alpha_g\rho_g v_g\omega_i\right)=\frac{\partial}{\partial z}\left(\alpha_g\rho_g D_{g,i}\frac{\partial\omega_i}{\partial z}\right)+\nu_i M_i r \quad (12)$$

The governing equations for the solid phase are the following:

Solid phase mass balance

$$\frac{\partial}{\partial t}\left(\alpha_p\rho_p\right)+\frac{\partial}{\partial z}\left(\alpha_p\rho_p v_p\right)=\Gamma+\sum_j r_j\sum_{i\in p}\nu_{i,j}M_i \quad (13)$$

Solid phase momentum balance

$$\frac{\partial}{\partial t}\left(\alpha_p\rho_p v_p\right)+\frac{\partial}{\partial z}\left(\alpha_p\rho_p v_p v_p\right)=-G\frac{\partial\alpha_p}{\partial z}-\alpha_p\frac{\partial p_g}{\partial z}$$
$$+\frac{\partial}{\partial z}\left(\alpha_p\mu_p^{eff}\frac{\partial v_p}{\partial z}\right)-\alpha_p\rho_p g+\beta\left(v_g-v_p\right)-\frac{2f_p\alpha_p\rho_p|v_p|v_p}{d} \quad (14)$$

Solid phase energy balance

$$\left(\frac{\partial T_p}{\partial t}+v_p\frac{\partial T_p}{\partial z}\right)\alpha_p\rho_p Cp_p=\frac{\partial}{\partial z}\left(\alpha_p\lambda_p\frac{\partial T_p}{\partial z}\right)-\Delta H r+a_s\alpha_p h\left(T_g-T_p\right)$$
$$+\frac{4}{d}h_{bed}\left(T_{wall}-T_p\right)+\int_{T_p}^{T_p'}\Gamma Cp_p(T_p')\,d(T_p'-T_p) \quad (15)$$

Solid phase species mass fractions

$$\frac{\partial}{\partial t}\left(\alpha_p\rho_p\omega_i\right)+\frac{\partial}{\partial z}\left(\alpha_p\rho_p v_p\omega_i\right)=\frac{\partial}{\partial z}\left(\alpha_p\rho_p D_{p,i}\frac{\partial\omega_i}{\partial z}\right)+\nu_i M_i r+\Gamma\omega_{i'} \quad (16)$$

Closures employed in this model are the ideal gas law for gas density and the constant particle viscosity model for the stresses. A list of constitutive relationships employed can be found in previous work (Sánchez et al. 2012). Properties with interfacial coupling, i.e. velocity and temperature, are solved together using the Partial Elimination Algorithm and a coupled solver. The SIMPLE algorithm for single phase flows is employed to calculate a pressure correction, modified to include the contribution of both phases.

The implementation of the coupling between units is done via source terms in the mass, energy and species mass fractions for the solid phase, i.e. the terms including Γ in (15) and (16).

Boundary and Initial conditions

On each unit Dirichlet boundary conditions are imposed for all variables except pressure at the inlet, while pressure is specified at the outlet. Neumann boundary conditions are specified for those variables that require a second boundary condition, e.g. velocities, temperature, etc.

The initial condition corresponds with minimum fluidization conditions. For most variables the initial condition is equal to the inlet boundary condition, e.g. for species mass fractions and temperatures. The initial condition for pressure is given by the hydrostatic distribution. The voidage at minimum fluidization can be found tabulated in the literature. The corresponding minimum fluidization velocity can then be calculated extrapolating the Ergun equation for pressure drop in a fixed bed.

In the SE-SMR simulations, the reformer is allowed to lose heat to the surroundings with a zero-dimensional model of a reactor wall made of stainless steal. The reactor wall transfers heat to the surroundings via natural convection and radiation. The wall of the regenerator unit

is heated at a constant temperature 50 ºC above the initial temperature for the regenerator.

Numerical algorithm

An overview of the solution algorithm is outlined below for the first of the units. The second unit is calculated after the first one, but without calculating the solid coupling source terms and solid mass fluxes, since they have been already determined for the current time step. The new values of velocity, species mass fractions, temperature and void fraction will be used in the next time step for the solid coupling source terms.

I. Update of inlet gas velocity and composition.
II. Reaction rates calculation.
III. Coupling source terms calculation.
IV. Gas phase species mass fractions.
V. Gas phase density update to account for changes in the gas composition.
VI. Temperature: Iteration loop comprising the calculation of all the temperature-dependent parameters, including Cp, viscosity and heat transfer coefficients. Inside the loop is also the calculation of the wall temperature.
VII. Gas phase density update to account for changes in the gas phase temperature.
VIII. An iteration loop comprising the following three iteration loops:
    a. Loop comprising void fraction and recalculation of the solids coupling source terms.
    b. Loop comprising velocities, viscosity, drag and friction factors.
    c. Loop comprising the solid phase species mass fractions, the recalculation of the solids coupling source terms and the solid density.
IX. Pressure correction
X. Velocities correction
XI. Gas phase density update due to a change in pressure

Cold flow validation

The hydrodynamics have been validated in previous work (Sánchez et al. 2012), where the expansion of the bed of solids was compared at different gas velocities against data from the literature measured using a radioactive tracking technique. The model and the data from the experiments were found to be in good agreement.

Reaction kinetics

The reforming reactions for commercial catalysts are taken from the work of Xu and Froment (1989). The CO2 sorption kinetics are taken from Sun et al. (2008) who provide data for both dolomite and limestone. Decarbonation kinetics from Okunev et al. (2008) are employed.

Chemical Looping Combustion kinetics have been investigated by various authors (Zafar et al. 2007, Adanez et al. 2012, Dueso et al. 2012), but the kinetics presented only consider the reduction of the oxygen carriers, without any analysis of the reforming that takes place due to the catalysing activity of the reduced oxygen carrier. Only recently this phenomenon has been investigated (Iliuta et al. 2010, Ortiz et al. 2012). Kinetics from Ortiz et al. are employed in this model.

RESULTS AND DISCUSSION

Arstad et al. (2012) conducted SE-SMR experiments in a CFBR during 8 hours of continuous operation and studied the dependence of the process upon the volumetric sorbent to catalyst ratio λ_{sc}, conducting experiments for λ_{sc} =1:1 and 1:4. In the present work it is aimed to reproduce their system and compare results for λ_{sc} =1:1, 1:2 and 1:4. The main parameters of this case are shown in Table 1.

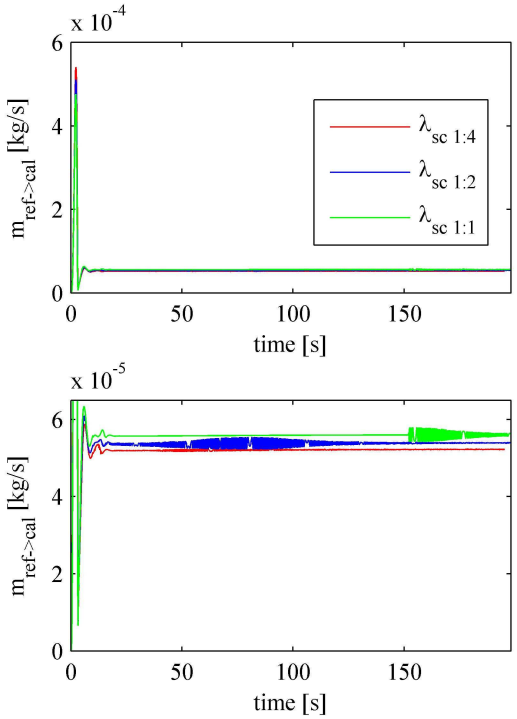

Figure 2a: Solid stream leaving the reformer and entering into the calciner. The bottom figure shows in more detail the different λ_{sc}.

Target mass stream between units	3.6 mL/min
Particle diameter	150 µm
CaO purity	51.5%
Bulk density fresh sorbent	830 kg/m^3
Bulk density catalyst	1040 kg/m^3
Initial temperature reformer	575 ºC
Initial temperature regenerator	895 ºC
Steam-to-carbon molar ratio	4
Internal diameter of both units	0.05 m
Reactor volume	182 mL
Mole fraction N_2 in the reformer	0.9
Mole fraction N_2 in the regenerator	1

Table 1: Parameters of the SE-SMR case studied.

Results for the solid streams exchanged between the units are shown in Figure 2. Arstad et al. diverted the solid flux into a measuring vial and reported that the solid streams between units were between 5 and 15 mL/min, but they acknowledge that it could have been as low as 3.6 mL/min based on ulterior calculations. In the simulations, the target solid stream was set to 3.6 mL/min and it was imposed via a control loop for the gas phase inlet velocity, which is shown in Figure 3. The corresponding target

solid stream is thus ~5.5×10^{-5} kg/s, depending slightly upon solid composition.

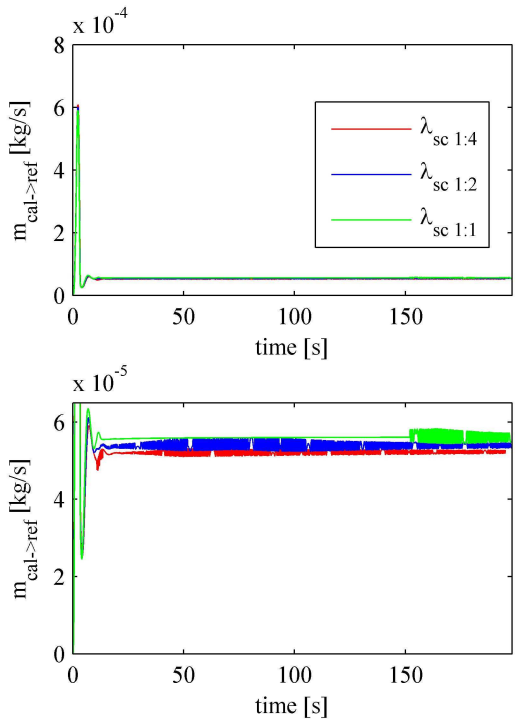

Figure 2b: Solid stream leaving the calciner and entering into the reformer. The bottom figure shows in more detail the different λ_{sc}.

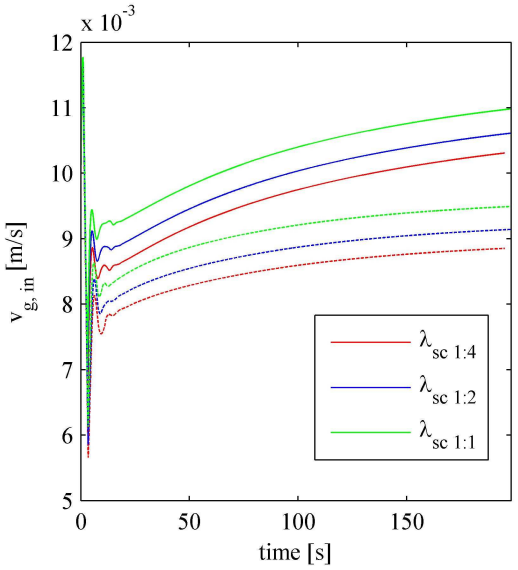

Figure 3: Gas phase inlet velocity. Full lines represent the reformer while dashed lines represent the calciner.

Inlet velocities from Figure 3 are higher for the cases with particles having a larger catalyst fraction. This is consistent with the fact that particles with larger densities need higher gas velocities to provide enough drag force to fluidize them. The catalyst has a larger density than fresh sorbent, as shown in Table 1.

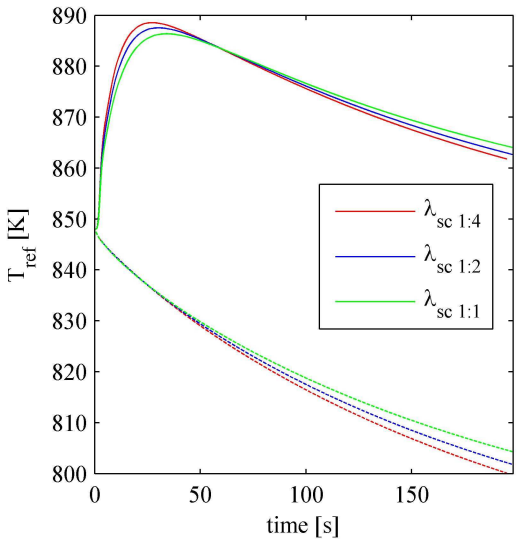

Figure 4: Temperature on the reformer. Full lines represent the average temperature of the solids, while the dashed lines represent the temperature at the wall.

The average temperature of the solids in the reformer is shown in Figure 4, along with the temperature of the reformer wall, plotted with a dashed curve.
The temperature rises due to the incoming solids from the calciner. In the same manner, the average temperature on the calciner drops due to the colder solids coming from the reformer, shown in Figure 5.
In the literature, the temperature on each unit is reported to remain close to initial values, but being unstable during the first hour of operation.

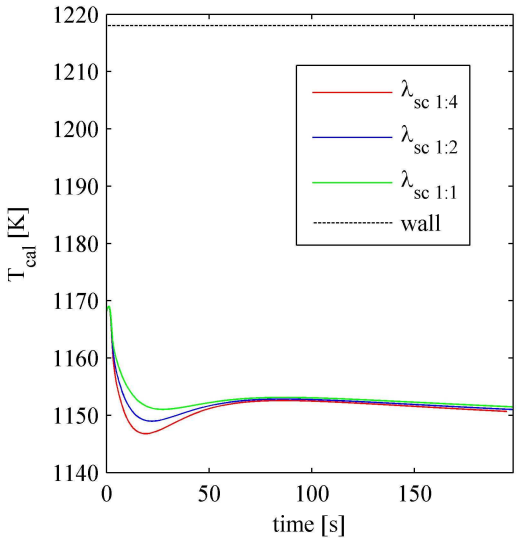

Figure 5: Temperature on the regenerator (calciner). Full lines represent the average temperature of the solids, while the dashed lines represent the temperature at the wall, which is constant and has the same value for all cases.

The present model does not consider the thermal capacity of the reactor components other than the reformer wall. In practise, the reactor components act as increased heat capacity and increased surface area for heat exchange with the surroundings, thus modifying the heat capacity and

thermal inertia of the system. These phenomena could be included in the numerical model by adding an extra heat capacity in parallel to the solids heat capacity, once these effects are empirically quantified.

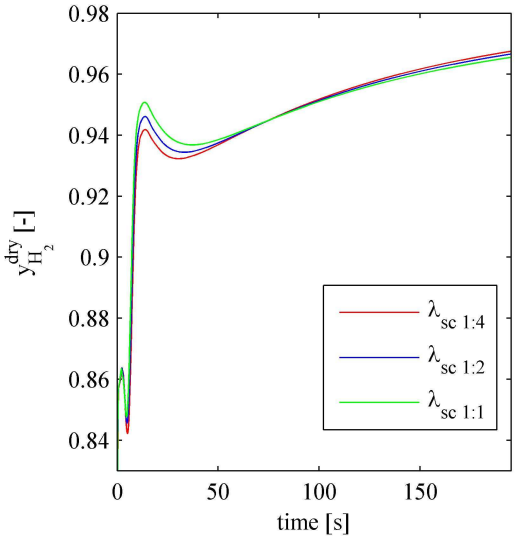

Figure 6: Hydrogen yield.

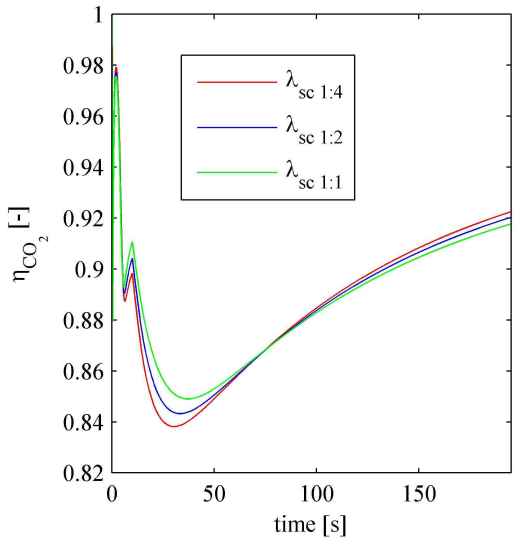

Figure 7: Instantaneous CO_2 capture efficiency.

The H_2 yield (the hydrogen mode fraction after subtracting nitrogen and steam) is plot in Figure 6, the instantaneous CO_2 capture efficiency is shown in Figure 7 and the CH_4 conversion is presented in Figure 8. These variables are defined in (17), (18) and (19) as

$$y_{H_2} = \left. \frac{y_{H_2}}{1 - y_{H_2O} - y_{N_2}} \right|_{outlet} \tag{17}$$

$$\eta_{CO_2} = 1 - \frac{\left. y_{CO_2} \right|_{outlet}}{\left. y_{CH_4} \right|_{inlet} - \left. y_{CH_4} \right|_{outlet}} \tag{18}$$

$$\eta_{CH_4} = 1 - \frac{\left. y_{CH_4} \right|_{outlet}}{\left. y_{CH_4} \right|_{inlet}} \tag{19}$$

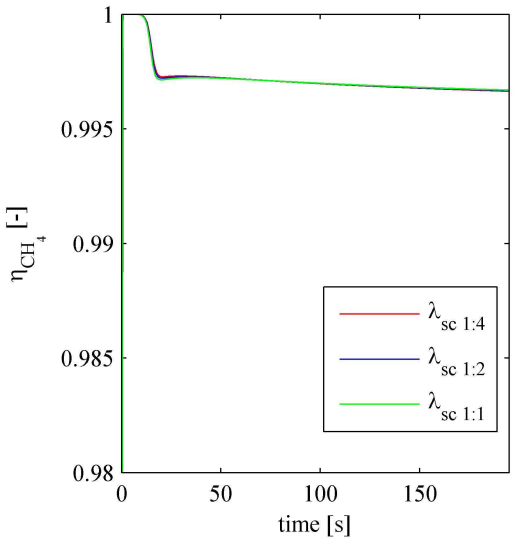

Figure 8: CH_4 conversion.

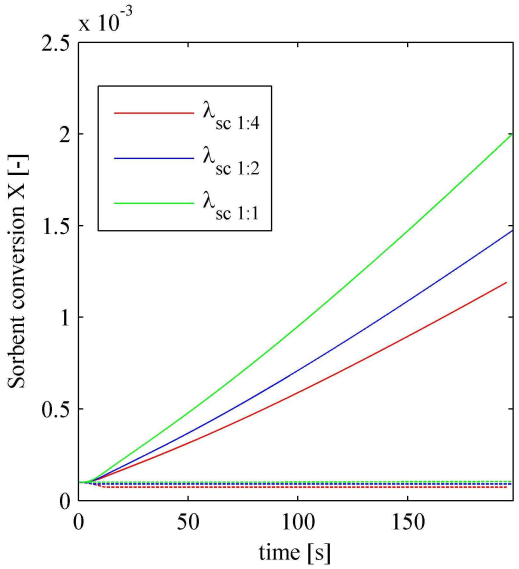

Figure 9: Sorbent conversion on each unit. Full lines represent the reformer while dashed lines represent the calciner.

Values reported in the literature are above 94% for H_2 yield and methane conversion, and between 60-90% for CO_2 capture efficiency.

Sorbent conversion X is plotted in Figure 9. It can be defined as the fraction of calcium-containing species which are present in the form of calcium carbonate. Since all the λ_{sc} cases studied have a similar CO_2 capture efficiency, the sorbent conversion X in the reformer must increase faster for the cases with larger catalyst content, because there is less sorbent present in the solids. The conversion in the calciner remains close to zero for all cases.

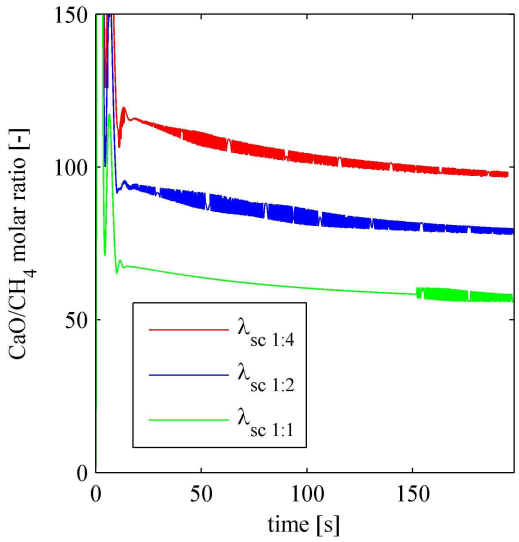

Figure 10: CaO to CH_4 molar ratio fed to the reformer. There is a peak off scale on the first seconds due to the peak in Figure 2b.

Figure 10 shows the ratio between the moles of CaO and the moles of CH_4 entering the reformer unit. Values above unity would ensure that there is enough sorbent present to capture all CO_2 produced, provided that the sorbent capacity is close to unity, i.e. the sorbent is fresh. It can be seen from the figure that all cases have enough sorbent to capture the maximum amount of CO_2 possible to create.

CONCLUSION

A CFBR model for the SE-SMR and the CLR processes is presented. The governing equations are solved for both phases, unlike the Kunii-Levenspiel type of models that assume stagnant solids. This is key to calculate solid streams exchanged between units of a CFBR.

Three cases with different λ_{sc} were reproduced numerically, and all three cases produced similar results for a time span analysed of ~200 s. Temperatures, solid mass streams, hydrogen yield, sorbent conversion, CH_4 conversion and CO_2 capture efficiency are plotted as a function of time.

Temperature profiles in the reformer are within 850 and 900 K, which is an optimal temperature range for SE-SMR. The reforming reactions are unfavoured below these temperatures, but still remaining below the equilibrium temperature for carbonation-decarbonation.

The results are in good agreement with the case with $\lambda_{sc\ 1:1}$ from the literature. The case with $\lambda_{sc\ 1:4}$ exhibited slightly higher hydrogen yield and smaller sorbent conversion, with these differences increasing towards the end of the simulations. This would suggest that the case with $\lambda_{sc\ 1:4}$ is preferable, since it features a higher H_2 yield and requires less catalyst, more expensive than calcium carbonates.

However, Arstad et al. obtained unexpectedly low hydrogen yields with $\lambda_{sc\ 1:4}$, between 80% and 10%, much smaller than for $\lambda_{sc\ 1:1}$. A possible cause is catalyst deactivation, not taken into account in the present work.

Longer simulation times are in any case needed for further studying the process and its dependence upon λ_{sc}, as well as the addition of a simple model to account for catalyst deactivation. That would permit analysing long-term effects, such as the influence of sorbent deactivation on the selection of an optimal value for λ_{sc}.

It is noted that in all cases simulated the CaO to CH_4 ratio was well above unity. As a consequence, all cases presented high CO_2 capture efficiency and H_2 yield. It is then predicted that other λ_{sc} values with less content of catalyst would still have produced high H_2 yields. It is therefore suggested that when calculating the optimal parameters for a given reforming system, all three λ_{sc}, the CaO to CH_4 ratio and the solid streams should be considered together, since they influence mutually.

Finally, the model presented is deemed useful for SE-SMR and future CLR simulations.

ACKNOWLEDGEMENTS

This publication has been produced with support from the BIGCCS Centre, performed under the Norwegian research program Centres for Environment-friendly Energy Research (FME). The authors acknowledge the following partners for their Contributions: Aker Solutions, ConocoPhilips, Det Norske Veritas AS, Gassco AS, Hydro Aluminium AS, Shell Technology Norway AS, Statkraft Development AS, Statoil Petroleum AS, TOTAL E&P Norge AS, GDF SUEZ E&P Norge AS and the Research Council of Norway (193816/S60).

REFERENCES

ADÁNEZ, J. et al., (2012), "Progress in chemical-looping combustion and reforming technologies", *Progress in Energy and Combustion Science Journal*, **38**, 215-282.

ARSTAD, B. et al., (2012), "Continuous hydrogen production by sorption enhanced steam methane reforming (SE-SMR) in a circulating fluidized bed reactor: sorbent to catalyst ratio dependencies", *Chemical Engineering Journal*, **189-190**, 413-421.

DUESO, C. et al., (2012), "Reduction and oxidation kinetics of nickel-based oxygen-carriers for chemical-looping combustion and chemical-looping reforming", *Chemical Engineering Journal*, 188, 142-154.

ILIUTA, I et al., (2010), "Chemical-looping combustion process: Kinetics and mathematical modeling", *AIChE Journal*, **56**, 1063-1079.

JAKOBSEN, H.A., (2008), "Chemical reactor modeling – Multiphase reactive flows", Springer.

OKUNEV, A.G. et al, (2008), "Decarbonation rates of cycled CaO sorbents", *Energy & Fuels*, **22**, 1911-1916.

ORTIZ, M. et al., (2012), "Catalytic activity of Ni-based oxygen carriers for steam methane reforming in chemical-looping processes", *Energy & Fuels*, **26**, 791-800.

SÁNCHEZ, R.A. et al., (2012), "Modeling and simulation of cold flow fluidized bed reactors", *Energy Procedia.*

SUN, P. et al., (2008), "Determination of intrinsic rate constants of the CaO-CO_2 reaction", *Chemical Engineering Science*, **63**, 47-56.

XU, J. and FROMENT, G.F., (1989), "Methane steam reforming, methanation and water gas shift: I. Intrinsic kinetics" *AIChE Journal*, 35, 88-96.

ZAFAR Q. et al., (2007), "Reaction kinetics of freeze-granulated NiO/MgAl2O4 oxygen carrier particles for chemical-looping combustion", *Energy & Fuels*, 21, 610-618.